Bragg Mirror Design for Optically Pumped Semiconductor Disk Lasers Emitting at 920 nm

Alexander Hein and Frank Demaria

Bragg mirror designs for Optically Pumped Semiconductor Disk Lasers (OPSDLs) are presented. An optimization takes into account parameters such as reflectivity, thermal resistance, and strain. Calculations and first results are shown for devices with an emission wavelength of 920 nm. The wavelength is of particular interest since its second-harmonic yields 460 nm emission required for RGB display applications.

1. Introduction

Within the last decade, OPSDLs experienced a drastic boost. These devices cover wavelengths from the UV to the IR and are capable of delivering output powers in the watt level for most of these wavelengths [1]. Naturally, there is a demand for a high material quality and for an elaborated layer design in order to overcome degradation mechanisms and to assure extended lifetime.

2. Mirror Type and Material

OPSDLs can be regarded as an active region with an integrated mirror. Since they are low gain devices, the quality factor of the resonator has to be rather high. The integrated mirror, a Distributed Bragg Reflector (DBR), should provide a reflectivity $\geq$ 99.9 %. Taking into account the output characteristics of the OPSDLs, higher outcoupling efficiencies are always achieved for higher reflectivities of the integrated mirror [2] as depicted in Fig. 1.

Highly efficient devices [3, 4] make use of so-called Double-Band Bragg Reflectors (DBBRs), providing a high reflectivity for the pump wavelength in addition to the high reflectivity for the emission wavelength. A benefit of such mirrors is the more homogeneous pumping of the Quantum Wells (QWs) since the profile of the pump intensity is primarily governed by a standing wave distribution and only marginally by the exponential decay being the case for single-band reflector structures. A further advantage is the recycling of the pump light which is not absorbed on a single pass, thus reducing the heat contribution in the reflector. OPSDLs with emission wavelengths related to InGaAs/GaAs-QWs (900–1200 nm) typically utilize DBBRs based on the well characterized $Al_xGa_{1-x}As$ alloy with the most common composition of $Al_{0.2}Ga_{0.8}As$/AlAs. In addition to the demand for high reflectivity, designs of DBBRs also strongly depend on the chosen thermal management approach. Utilizing transparent intra-cavity heat spreaders such as diamond or

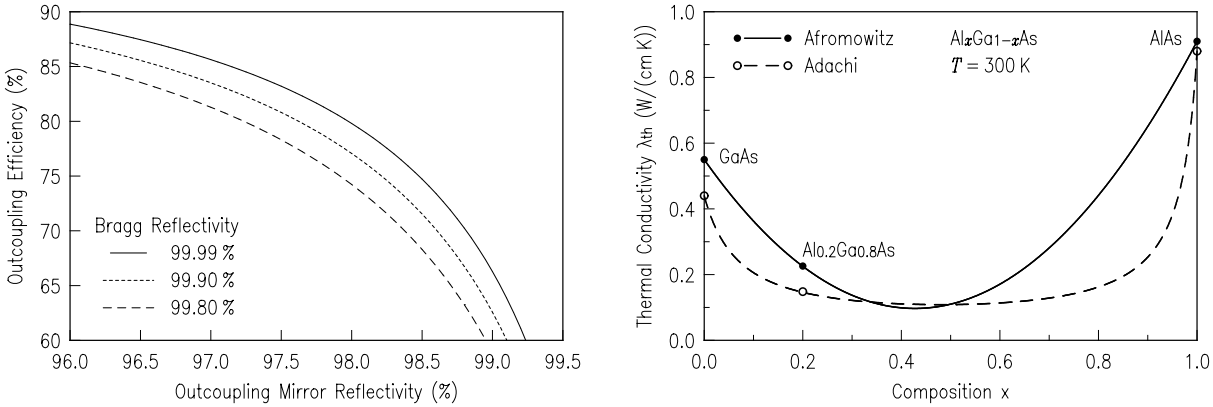

Fig. 1: Outcoupling efficiency for different Bragg mirror reflectivities (left) and thermal conductivity of the $Al_xGa_{1-x}As$ alloy (right) according to [7, 8].

silicon carbide [5], optimization of the thermal resistance of the mirror is not necessary since the largest amount of produced waste heat simply bypasses the DBBR. However, when the more cost effective thin device approach is chosen, where the laser is grown as a bottom emitter and the substrate is removed in postprocessing, the thermal resistance of the mirror should be minimized, simultaneously maintaining the high reflectivity.

3. Mirror Designs

3.1 Thermal considerations

The quantum defect for barrier pumped devices emitting at 920 nm – accounting for the typical pump wavelength of around 808 nm – is rather small compared to longer wavelength OPSDLs. However, a major challenge for the emission at 920 nm is the carrier confinement at elevated temperatures and carrier spillover at high injection levels due to the small energy difference between the InGaAs QW and GaAs barrier ($\approx$ 80 meV) [6]. The layer design of the Bragg mirror is considered with the focus on the reduction of the thermal resistance. An easy approach is to exploit the material system. As shown on the right side of Fig. 1, the AlAs layers of an $Al_{0.2}Ga_{0.8}As$/AlAs Bragg mirror have significatly higher thermal conductivity. Therefore, AlAs is used for the thicker phase matching layers needed for the dual wavelength mirrors. Figure 2 shows the calculated reflectivities of DBBRs with equal thickness, where one structure is a standard approach and the other structure incorporates the described feature. The thermal resistivity of each layer is calcultated according to

$$R_{\mathrm{th},i} = \frac{t_i}{\lambda_{\mathrm{th},i}}, \tag{1}$$

where t_i is the respective layer thickness and $\lambda_{\mathrm{th},i}$ is the temperature-dependent thermal conductivity for the $Al_xGa_{1-x}As$ alloy [8] given by

$$\lambda_{\mathrm{th}} = \frac{1}{xW_{\mathrm{GaAs}} + (1-x)W_{\mathrm{AlAs}} + x(1-x)C_{\mathrm{Ga-Al}}}, \tag{2}$$

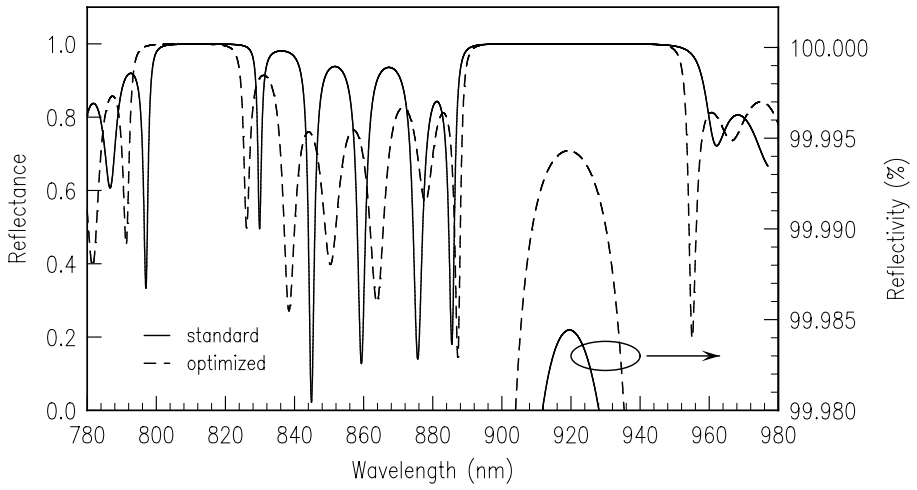

Fig. 2: Calculated reflectivity characteristics of double band Bragg reflectors for a standard and thermally optimized design.

where W_{GaAs} and W_{AlAs} are the binary thermal resistivities, and $C_{\mathrm{Ga-Al}}$ is a disorder factor. The overall thermal resistivity of the multilayer system is calculated from the series connection of the single thermal resistivities:

$$R_{\mathrm{th,tot}} = \sum_i R_{\mathrm{th},i} = \sum_i \frac{t_i}{\lambda_{\mathrm{th},i}}. \tag{3}$$

The described structures are compared in terms of their thermal resistivity according to the above equations in Fig. 3. For the structures under investigation the layer resistivities were calculated as $0.233\,\mathrm{K}\cdot\mathrm{mm}^2/\mathrm{W}$ and $0.168\,\mathrm{K}\cdot\mathrm{mm}^2/\mathrm{W}$, respectively. For typical pump spots of 300 µm diameter the thermal resistance would account to 3.29 K/W and 2.38 K/W, equivalent to an improvement of 18 %.

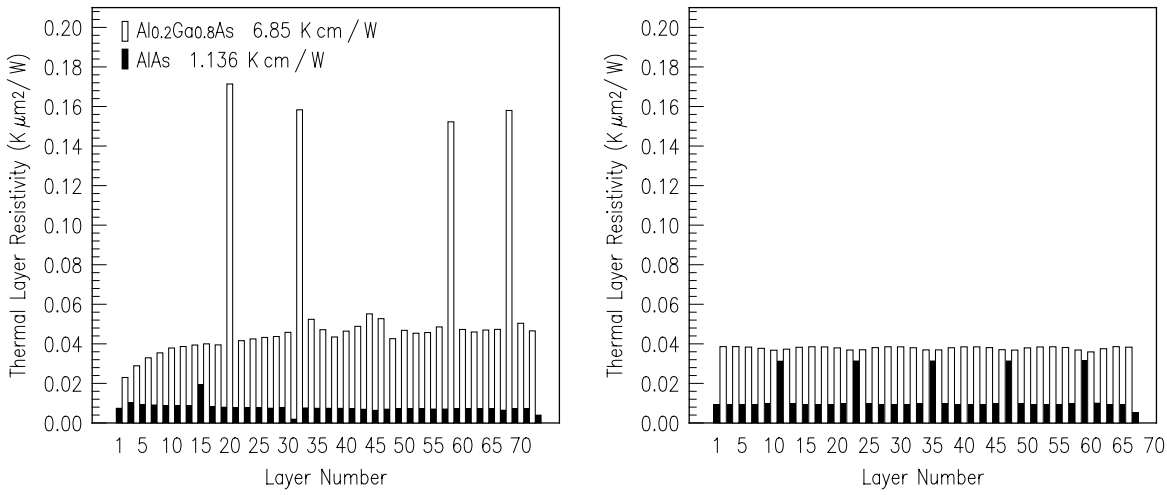

Fig. 3: Thermal layer resistivities of a standard (left) and thermally optimized structure with high AlAs content (right).

3.2 Strain considerations

A major shortcoming utilizing thick AlAs layers arises from the larger strain incorporation. Experiments revealed degradation of the thermally optimized samples, especially when values for the critical thickness in single layers were exceeded, as illustrated in Fig. 4.

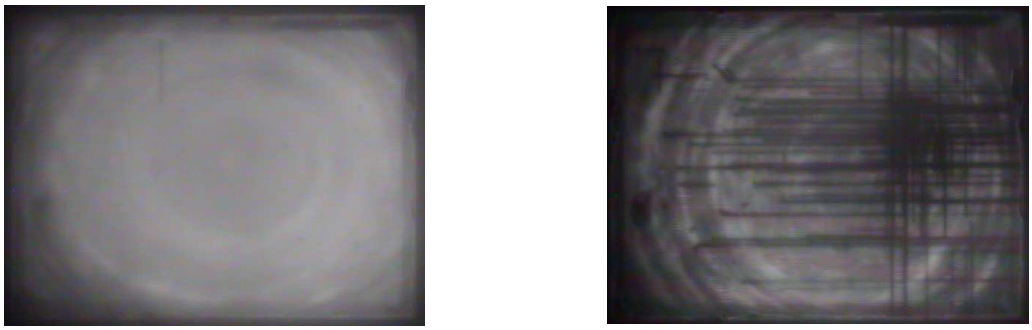

Fig. 4: Locally resolved photoluminescence images of the thermally optimized sample before (left) and after (right) laser operation. The sample was illuminated with a pump laser diode emitting at 808 nm.

A simple qualitative comparison between the structures regarding strain can be drawn weighting the energy stored in the respective structures. The stored energy of a multilayer system can be calculated according to

$$W_{\mathrm{tot}} = \sum_i W_i = \sum_i C_i t_i \epsilon_{||\,i}^2, \tag{4}$$

where $\epsilon_{||\,i}$ is the in-plaine strain given by the mismatch to the substrate and C_i represents the elastic constant of the respective materials [9]. A comparison between the standard and thermally optimized design is depicted in Fig. 5.

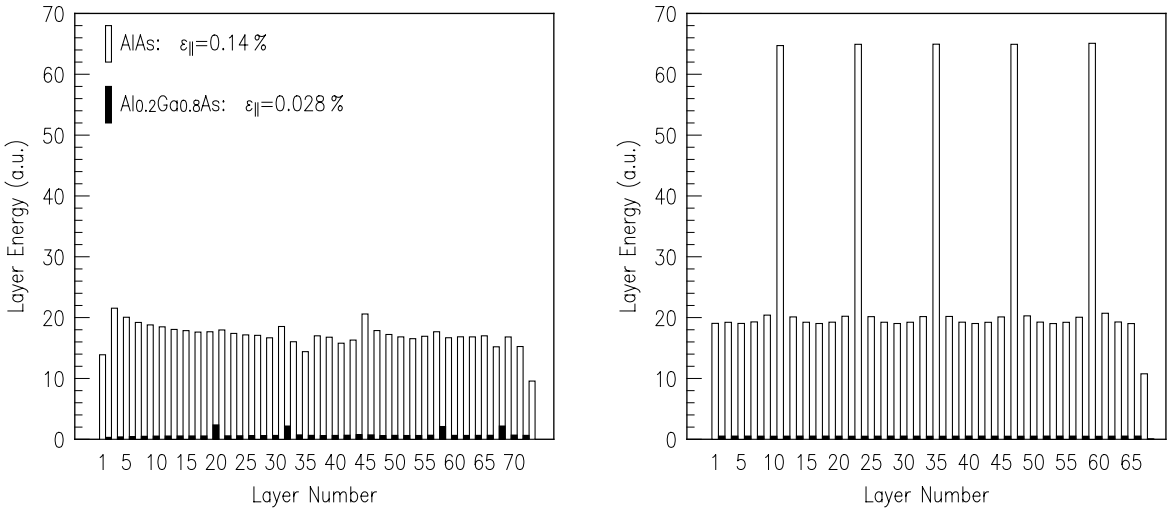

Fig. 5: Comparison of the strain incorporation by means of the respective layer energies of a standard structure (left) and one with higher AlAs content (right).

The highest strain contribution results from the thick AlAs layers. Even though the critical thickness can be exceeded without the formation of dislocations [9], the thick AlAs layers are a weak spot because the single layers already exceed the critical thickness during growth when the structure is susceptible. As described in [10] a straightforward approach would be to replace the adjacent $Al_{0.2}Ga_{0.8}As$ layers by $GaAs_{0.8}P_{0.2}$. In general, with typical layer thicknesses slightly varying around one Quarter Wave Optical Thickness (QWOT) it is not possible to simply replace $Al_{0.2}Ga_{0.8}As$ by $GaAs_{0.8}P_{0.2}$ without offending the critical thickness limitation for $GaAs_{0.8}P_{0.2}$ due to the high lattice mismatch ($\epsilon_{||}$=0.73 %). Hence, this single optical layer is in fact a two layer $Al_{0.2}Ga_{0.8}As$/GaAsP compound, where the phosphorus concentration must be set in a very precise way to match the refractive index of $Al_{0.2}Ga_{0.8}As$. This would introduce adverse conditions for the epitaxial growth. An alternative approach is a distributed compensation, where the thick AlAs layers are split by thin GaAsP intermediates. As shown in Fig. 6 the reflectivity characteristic is not impaired by this method but by proper positioning even slightly enhanced, and deviations of the phosphorus concentration are less crucial.

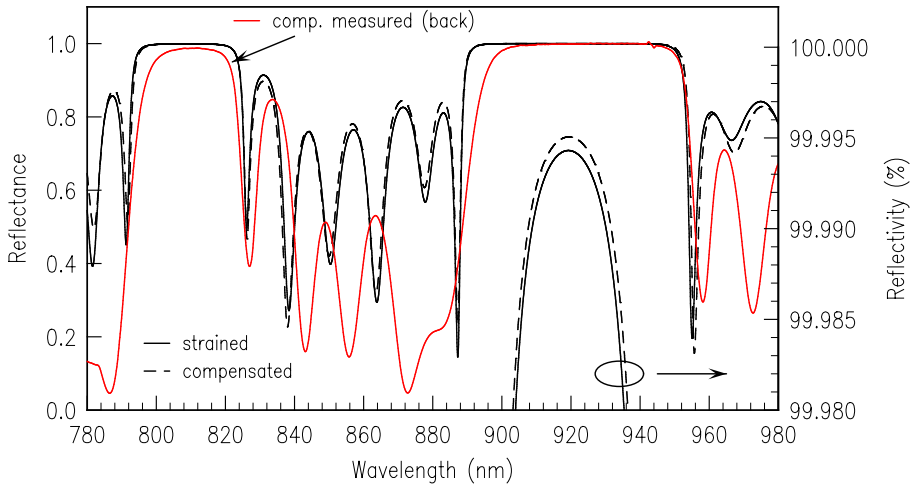

Fig. 6: Calculated reflectivities of structures without and with partial strain compensation, as well as a measured reflectivity characteristic for the compensated structure.

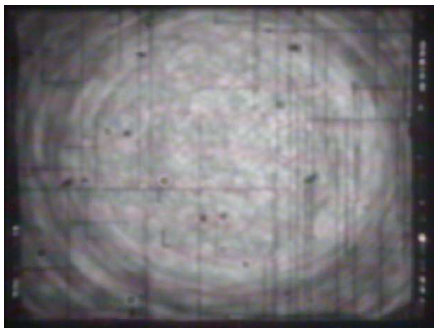

Fig. 7: Locally resolved photoluminescence image of a strain compensated structure, where dislocation defects are still clearly recognizable.

Refering to Fig. 7 a fully successful compensation utilizing the intermediate layer method was not achieved. Although degradation of the compensated structures was not observed,

the defects set a limit to the lasing perfomance. Possible options to further minimize the dislocation defects are higher phoshorus concentrations ($\geq 25\,\%$) in the compensating layers or a higher quantity of these. However, additional layers and interfaces subvert the thermal optimization, thus, a different approach is explored.

4. Hybrid Bragg Reflector

In order to reduce the limitations imposed by strain and simultaneously keeping the thermal resistance to a minimum, a hybrid mirror – combination of a double- and single-band mirror structure – with reduced AlAs content could be a promising approach. Here, a slightly lower reflectivity for the pump wavelength is traded for a thinner top DBBR structure. To maintain the high reflectivity for the emission wavelength the structure is completed with a bottom single-band mirror. The reflectivity characteristic is plotted in Fig. 8 in comparison with the designs described before.

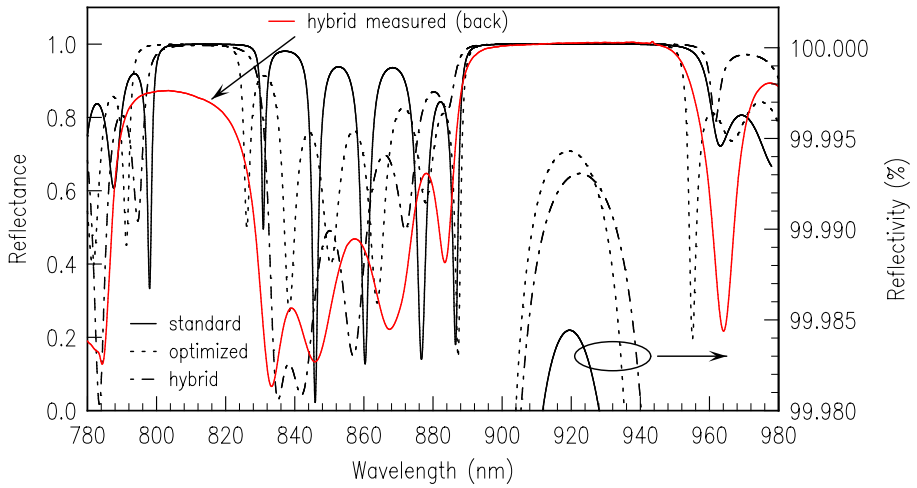

Fig. 8: Comparison of reflectivity characteristics for a hybrid structure with previously proposed designs. Measurement of the hybrid shows good agreement with the calculation except for the damped minor stop band which results from pump light absorption in the single-band mirror.

An argument in favour of such a structure is the possibility of using GaAs in the bottom reflector which due to the high absorption of the pump light normally cannot be employed in a DBBR. Further advantages are the innate better thermal conductivity compared to $Al_{0.2}Ga_{0.8}As$, a slightly reduced thickness due to a higher refractive index, and no strain contribution. It also seems advantageous to replace the high refractive index layers of $Al_{0.2}Ga_{0.8}As$ by $Al_{0.15}Ga_{0.85}As$ in the double-band part. In addition to an improvement of the thermal conductivity ($\approx 14\,\%$), a smaller lattice mismatch is noted. Taking into account the thermally induced shrinkage of the band gap of AlGaAs at the Γ-valley from the relation

$$E_\Gamma(T) = \left(1.7 - \frac{5.41 \cdot 10^{-4} \cdot T^2}{T + 204}\right) \text{ eV} \ , \tag{5}$$

the energy of $Al_{0.15}Ga_{0.85}As$ [11] is large enough to avoid absorption of pump light as long as the temperature is below 450 K. The comparison of thermal characteristics and strain evaluation are shown in Fig. 9.

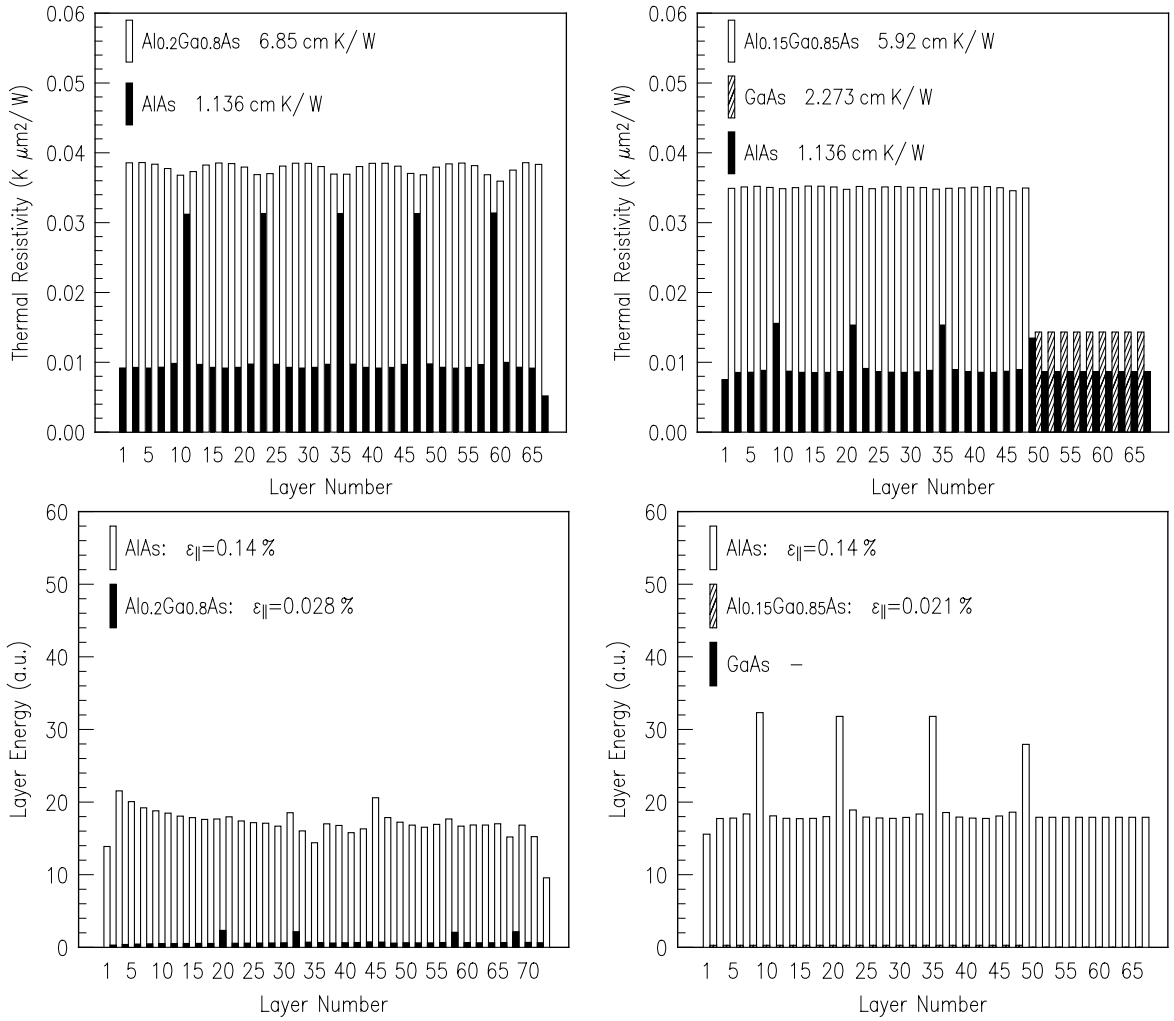

Fig. 9: Thermal resistivity and strain evaluation for the hybrid mirror (right-top and right-bottom) in a triangulation comparison. Thermal resistivity is compared to a thermally optimized structure (top left), whereas strain evaluation is refered to a standard design (bottom left).

Evaluation of the thermal resistance shows an improvement of 23 % (1.83 K/W) compared to the best thermally optimized DBBR structure. Moreover, calculation of the overall stored energy reveals a value which is only 1.3 % larger compared to the standard design.

5. Conclusion

To enhance OPSDL performance we presented new designs regarding the integrated double-band Bragg reflectors in terms of thermal optimization and structural stability. In particular, for the hybrid mirror approach there is an indication that for similar reflectivity behaviour, thermal characteristics clearly outperform standard structures as well

as structures with high AlAs contents for optimized thermal resistance. Regarding strain contribution the hybrid mirror performs equally to the strain proven standard devices and is to be employed in future OPSDL generations.

References

[1] S. Calvez, J.E. Hastie, M. Guina, O.G. Okhotnikov, and M.D. Dawson, "Semiconductor disk lasers for the generation of visible and ultraviolet radiation", *Laser and Photon. Rev.*, vol. 3, pp. 407–434, 2009.

[2] M. Kuznetsov, F. Hakimi, R. Sprague, and A. Mooradian, "Design and characteristics of high power (> 0.5-W cw) diode-pumped vertical-external-cavity surface-emitting semiconductor lasers with circular TEM_{00} beams", *IEEE J. Select. Topics Quantum Electron.*, vol. 5, pp. 561–573, 1999.

[3] F. Demaria, S. Lorch, S. Menzel, G. Riedl, F. Rinaldi, R. Rösch, and P. Unger, "Design of highly efficient high-power optically pumped semiconductor disk lasers", *IEEE J. Select. Topics Quantum Electron.*, vol. 3, pp. 973–977, 2009.

[4] A. Hein, F. Demaria, A. Kern, S. Menzel, F. Rinaldi, R. Rösch, and P. Unger, "Efficient 460-nm second-harmonic generation with optically pumped semiconductor disk lasers", *IEEE Photon. Technol. Lett.*, vol. 23, pp. 179–181, 2011.

[5] K. Kim, J. Yoo, G. Kim, S. Lee, S. Cho, J. Kim, T. Kim and Y. Park, "920-nm Vertical-external-cavity surface-emitting lasers with a slope efficiency of 58% at room temperature", *IEEE Photon. Technol. Lett.*, vol. 19, pp. 1655–1657, 2007.

[6] A.P. Ongstad, D.J. Gallant, and G.C. Dente, "Carrier lifetime saturation in InGaAs single quantum wells", *Appl. Phys. Lett.*, vol. 20, pp. 2730–2732, 1995.

[7] M.A. Afromowitz, "Thermal conductivity of $Ga_{1-x}Al_xAs$ alloys", *J. Appl. Phys.*, vol. 44, pp. 1292–1294, 1973.

[8] S. Adachi, "Lattice thermal conductivity of group-IV and III-V semiconductor alloys", *J. Appl. Phys.*, vol. 102, pp. 063502-1–063502-7, 2007.

[9] F. Rinaldi, *MBE growth and characterization of multilayer structures for vertically emitting laser devices*. Ph.D. thesis, Ulm University, Ulm, Germany, 2008.

[10] F. Rinaldi and S. Menzel, "Advanced strain compensation in MBE-grown semiconductor disk lasers", *Annual Report 2009*, pp. 11–16, Ulm University, Institute of Optoelectronics.

[11] Ioffe Physico-Technical Institute, "Electronic Archive: Physical Properties of Semiconductors", *http://www.ioffe.ru/SVA/NSM/Semicond/AlGaAs/index.html*, 2010.